Sensor and Simulation Notes

Note 299

01 April 1987

Early Time Performance at Large Distances of Periodic Arrays of Flat-Plate Conical Wave Launchers

D. V. Giri

Pro-Tech, 125 University Ave., Berkeley, California 94710

and

Carl E. Baum

Air Force Weapons Laboratory

ABSTRACT

This note is an extension of past work on this subject [1] which considered the performance of infinite planar arrays of interconnected planar biconical sources. In order to obtain an improved performance in the context of the rate of rise in the distant field, we have considered an array of conical wave launchers in this note. Formulae for the early-time rise of such arrays are developed, tabulated and plotted, as a function of normalized geometrical parameters of an individual launcher and the array.

CONTENTS

I. Introduction

Many techniques have been investigated for the purpose of launching transient electromagnetic (EM) waves and the results have been incorporated in the design of various categories of EMP Simulators [2]. One such technique involves configuring many sources into an array. The source array synthesizes an appropriate aperture field distribution to launch a desired type of wave. The individual sources are interconnected in some series-parallel fashion. The conducting surfaces that interconnect the modular sources have a significant impact on the early-time rate of rise in the distant field. Planar arrays [1,3] and non-planar arrays [4,5] have been considered in the past. In practice, the distributed source will have to be replaced by a discrete array of modular sources [6]. In this note, we are considering some possible geometries of unit cells in the distributed-source or distributed-switch [5] wave launchers. Attention is focussed on one aspect of performance, i.e., the rate of rise in the far field (for assumed ideal step-function sources) of candidate unit cell designs. The unit cells considered are planar-conical or non-planar wave launchers. While considering such non-planar arrays of wave launchers, the unit cell size is small compared to the array dimensions so that we can analyze the effects associated with the unit-cell design while letting the array be infinitely large. There are perhaps many module or unit-cell designs one may consider, each being associated with its own boundary value problem. Two illustrative examples are presented in this note.

After considering the unit cell properties and the general characteristics of conical wave launchers, we deal with the summation of early-time fields of unit cells to yield the early-time performance of the array. The precise fields on flat-plate cylindrical and conical transmission lines are reviewed leading to the early-time performance of an array of flat-plate conical transmission lines. The note is concluded with a summarizing section and an appendix with the numerical results for examples of unit-cell geometries.

II. Unit Cell Considerations

The basic electromagnetic problem under consideration is one of simulating a distributed source by an array of discrete generators. [6] considered the problem of approximating the source by a two-dimensional modular array with two possible design choices, viz, in-line configurations, and staggered configurations. These are schematically represented in figures 1 and 2. In the in-line configuration, PQRS is symbolically the unit cell with dimensions of $2a \times 2b$ and repeating itself in both series and parallel directions. In the case of staggered configurations, the adjacent series band or group of sources are displaced by an amount a, as seen in figure 2. One can heuristically argue that the staggered configuration has somewhat improved high frequency characteristics [6] at the aperture plane. However, at large distances this may not be the case as the results of this note indicate. It is noted that the two configurations of figures 1 and 2 are only schematic representations.

In practice, the individual source could be typically a capacitor and a switch close to the aperture plane. The conductors associated with each source are themselves interconnected so that currents can flow in the array resulting in the desired, non-zero, average tangential electric field in the aperture plane. Such an aperture field distribution then radiates efficiently at wavelengths large compared to the basic cell size. Baum [3] considered some characteristics of planar distributed sources for radiating transient fields, in a qualitative way pointing out many of the potential features of such arrays.

Recalling the present interest in a two-dimensional array of conical wave launchers, we need to formulate the relationships useful in quantitative estimation of the early-time performance from such an array of conical launchers. With this in mind, general characteristics of conical launchers are reviewed in the following section.
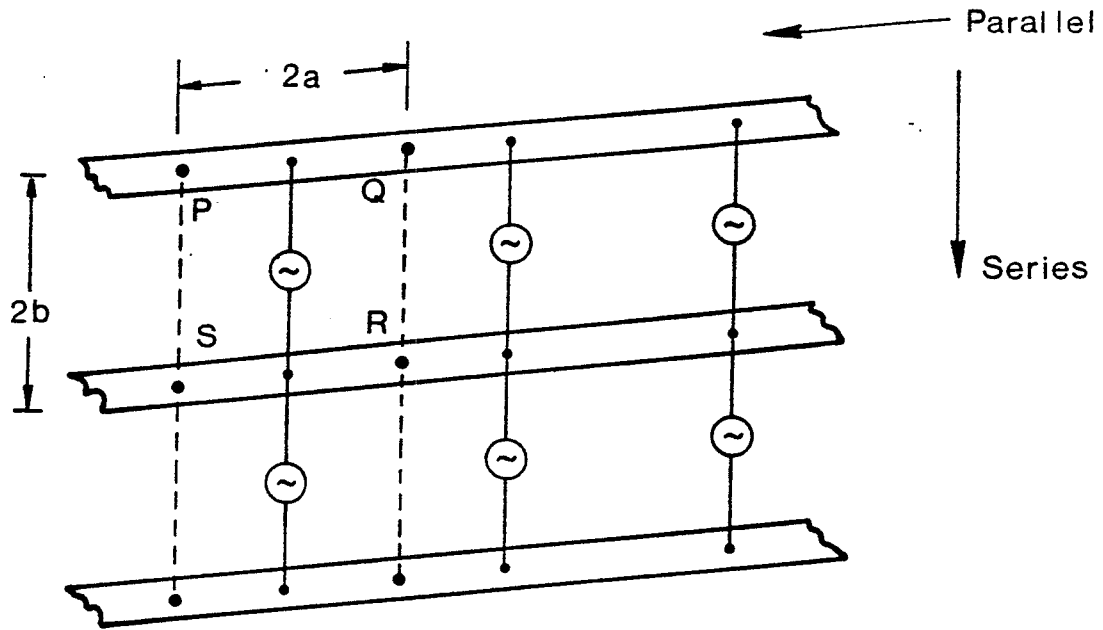
Figure 1. Schematic diagram of modular sources arranged in an in-line configuration
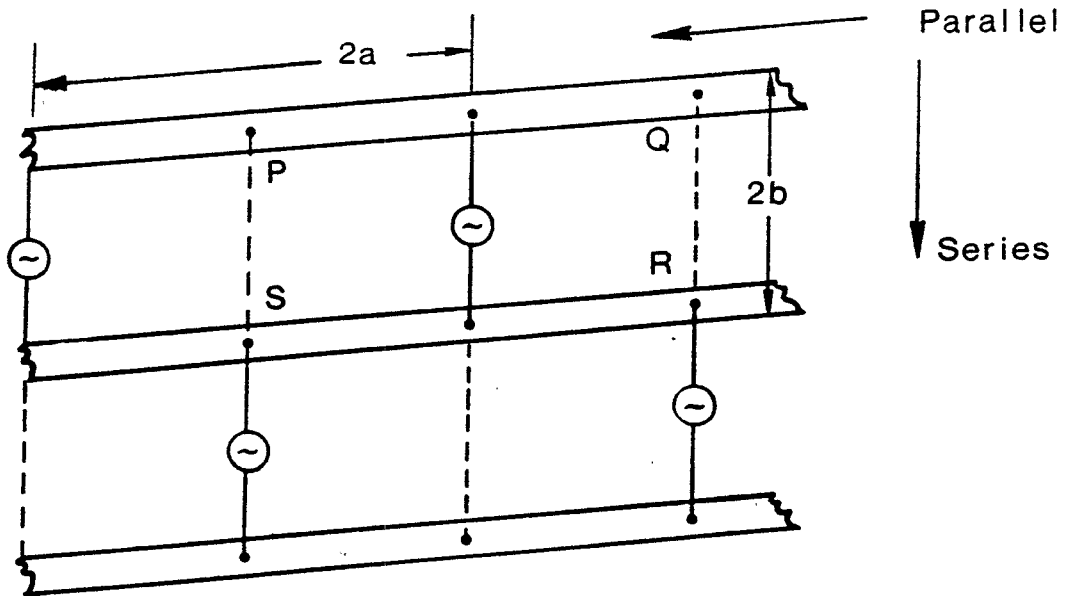
Figure 2. Schematic diagram of modular sources arranged in a staggered configuration

III. General Characteristics of Conical Launchers

In this section we consider some general performance characteristics of a spherical TEM element, i.e. conical launcher. For simplicity, one can consider a planar array of spherical TEM radiating elements as shown schematically in figure 3, and a spherical coordinate system with its origin at one of the reference points is indicated in figure 4. Each reference point lies in an area A ($= 4ab$ for the rectangular array shown), which is the area of the unit cell in an "infinite" array. Each source is assumed to launch the same type of wave and at the same time as every other source except for a translation in the source plane, resulting in a different arrival time at an observation point.

The spherical TEM wave launched from one reference point at $\vec{r} = \vec{0}$ in figure 4, under a step function assumption is of the form [7, 8 and 1]

$$\vec{E}(\vec{r},t) = -\frac{V_0}{r} \nabla_{sp} f(\theta,\phi)\, u\left[t - \frac{r}{c}\right] \tag{1}$$

This wave starts at $\vec{r} = \vec{0}$ at $t = 0$ and ∇_{sp} is the gradient on the unit sphere operating on the voltage function $f(\theta,\phi)$ according as

$$V(\vec{r},t) = V_0 f(\theta,\phi)\, u\left[t - \frac{r}{c}\right] \tag{2}$$

Substituting for the gradient, one can obtain

$$\vec{E}(\vec{r},t) = -\frac{V_0}{r} \vec{F}(\theta,\phi)\, u\left[t - \frac{r}{c}\right] \tag{3}$$

where

$$\vec{F}(\theta,\phi) = \nabla_{sp} f(\theta,\phi)$$

$$= \vec{1}_\theta \frac{\partial}{\partial\theta} f + \frac{1}{\sin(\theta)} \vec{1}_\phi \frac{\partial f}{\partial\phi} \tag{4}$$

Equation (3) displays the angular variation of the electric field via $\vec{F}(\theta,\phi)$ and it also shows the r^{-1} fall off in the distant field.
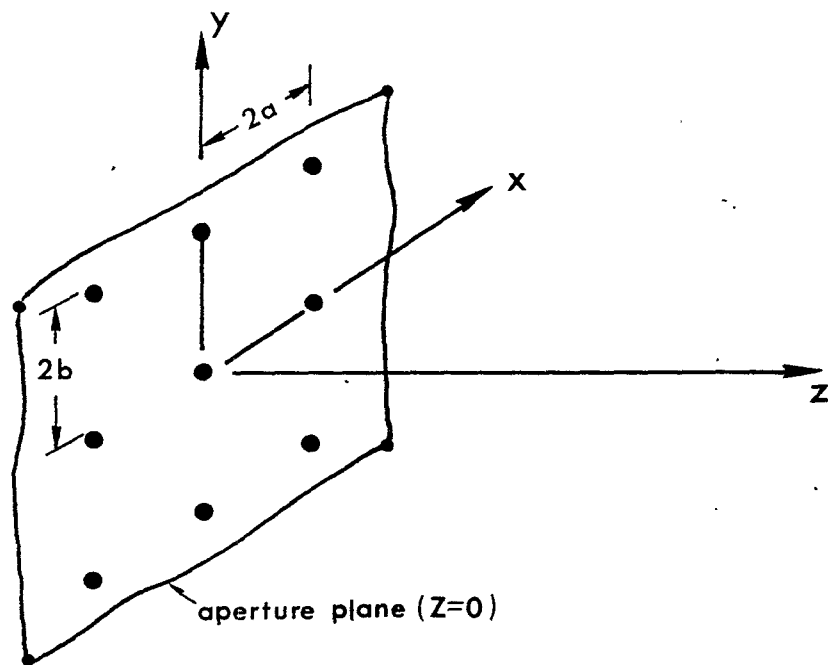
Figure 3. Rectangular array of spherical TEM elements
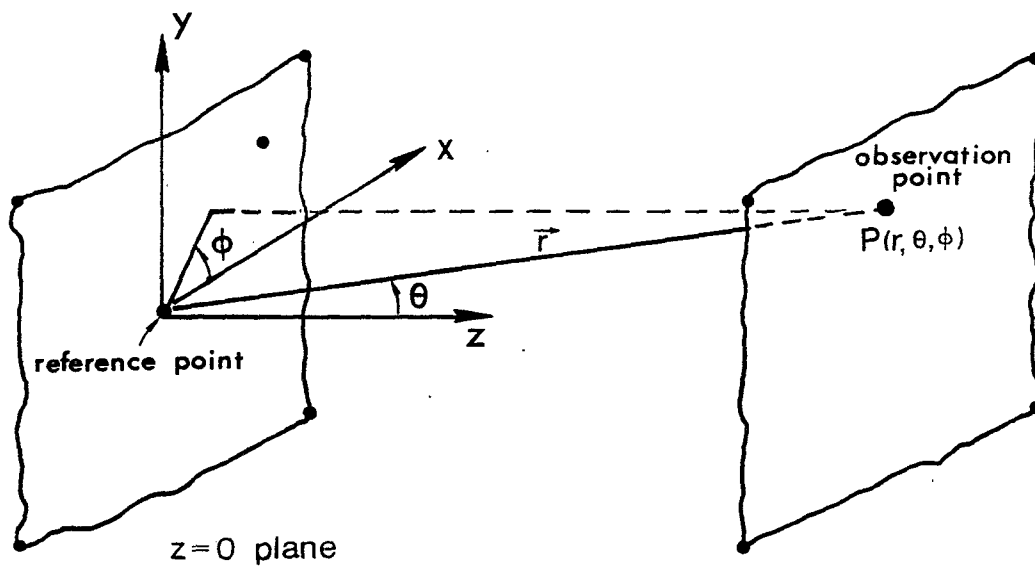
Figure 4. Spherical coordinates for the early-time field
distribution near a single element

The angular distribution of the electric field is postulated to be the same from all source points in the array except for their location, accounted later by a pair of indices n, m. Initially we will be considering a planar array of source points in the $z = 0$ plane.

IV. Early-Time Performance of the Array from the Early-Time Fields of Unit Cells

We turn our attention to the process by which the Fields from all elements of the array in the aperture plane at $z = 0$ combine to maintain the far field. With reference to figure 5, $z = 0$ is the aperture plane containing an array of spherical TEM elements. We seek to establish the time-dependent observer-sources relationship. In other words, a distant observer on the z axis, for example, sees the field first from the nearest source. Then as time progresses the observer sees all sources within a circle whose radius $R(t)$ is expanding in time according as [1]

$$R(t) = \sqrt{2rct_r}$$

$$t_r = t - \frac{r}{c} \tag{5}$$

and the time dependent area of this expanding circle is

$$A_1(t) = \pi \, 2rct_r \tag{6}$$

The number of sources seen by the observer is simply the above area divided by the area A of the unit cell so that the far field is,

$$\vec{E} = -\frac{V_0}{A} \left[\pi 2rct_r \right] \left[\frac{1}{r} \right] \vec{F}(0,\phi)\, u\,(t_r)$$

$$= -\frac{2\pi V_0}{A} (ct_r)\, \vec{F}(0,\phi)\, u\,(t_r) \tag{7}$$

This is a basic result for the planar array derived in a previous note [1], and specialized here for normal launch angle. It is interesting to note that if the array is truly infinite, the far field is independent of r for fixed retarded time t_r.

If one also looks at the late-time field and normalizes the far field to its late-time value [1] has shown that this ratio at early time is

$$\left[\frac{E_y \text{ (far field along the normal)}}{E_0 \quad \text{(late time value)}} \right] = 2\,\pi\, F_y(\theta,\phi)\, \frac{h}{A} ct_r\, u(t_r)$$

$h \equiv$ spacing between sources in the (8) of direction the electric field.
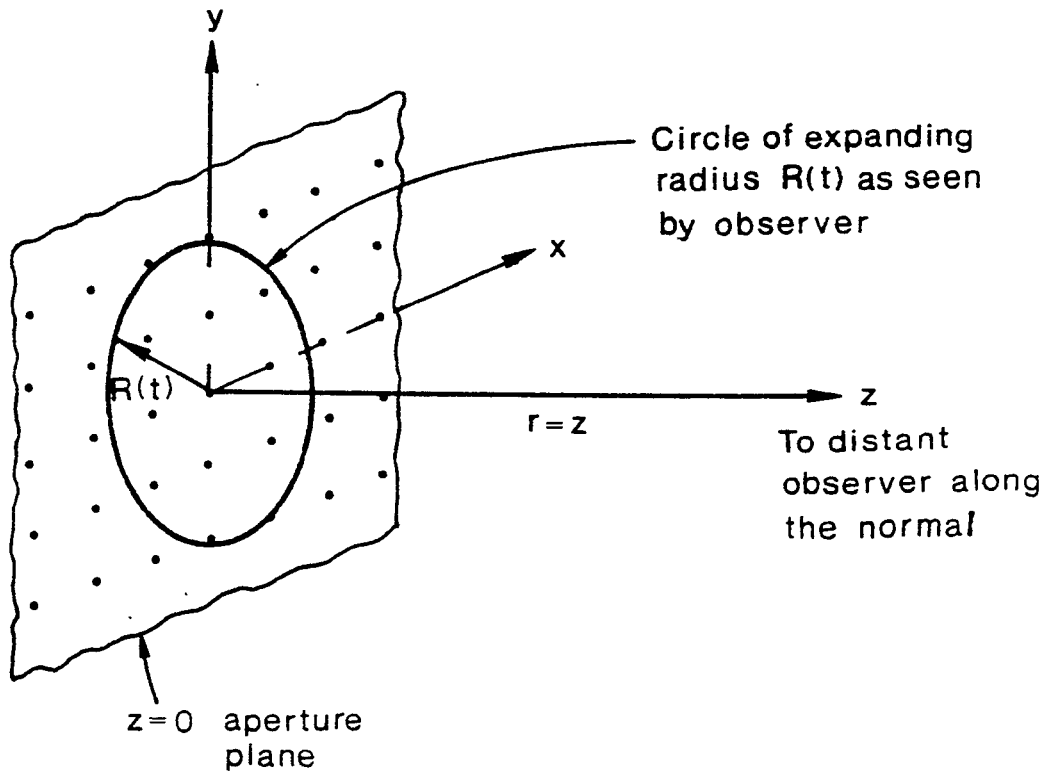
Figure 5. Observer — sources relationship
as time progresses

Setting this ramp function equal to 1 defines an effective rate of rise for early times as

$$t_1 = \frac{A}{2\pi ch} (F_y(\theta, \phi))^{-1} \qquad (9)$$

It remains to determine the functional form of $\vec{F}(\theta, \phi)$, which can be done as follows for an example geometry.

Now consider an array of conical wave launchers connecting source points (apices) behind the $z = 0$ plane to the $z = 0$ plane. For an observer in a direction normal to the aperture plane ($z = 0$), at a distance r measured from the aperture plane along the z axis as indicated in the side view of figure 6. Observe that the individual generators at or near the theoretical apices turn on at $t = -l/c$ so that the arrival time at the reference point is $t = 0$. The electric field at this special observation point along the z axis, in terms of the field at the reference point can then be written as

$$\vec{E}_1(\vec{r},t) = \frac{l}{r+l} \frac{V_0}{2b} u \left[t - \frac{r}{c} \right] \vec{E}_{rel} \qquad (10)$$

$\vec{E}_{rel}$ is a dimensionless field which indicates the electric field at the reference point under consideration normalized to the average field of $| V_0/(2b) |$. It is easily verified by letting $r = 0$ in the above that $\vec{E}_1$ reduces to the field at the reference point which is turned on at $t = 0$. The factor $[l/(r+l)]$ in front accounts for the $(1/r)$ fall off in the electric field. One can rewrite (10) as follows

$$\vec{E}_1(\vec{r},t) = \frac{1}{r+l} V_0 \left\{ \frac{l}{2b} \vec{E}_{rel} \right\} u \left[t - \frac{r}{c} \right]$$

$$= \frac{1}{r(1+\frac{l}{r})} V_0 \left\{ \frac{l}{2b} \vec{E}_{rel} \right\} u \left[t - \frac{r}{c} \right]$$

$$= \frac{V_0}{r} \left[1 + O(r^{-1}) \right] \left\{ \frac{l}{2b} \vec{E}_{rel} \right\} u \left[t - \frac{r}{c} \right] \qquad (11)$$

2a

Theoretical apex

y

b

$V_0 u\left(t + \dfrac{\ell}{c}\right)$
source

ℓ

x

The point of first
arrival at $t = 0$ in
the aperture plane from
a single TEM element

observer

z = 0
aperture plane
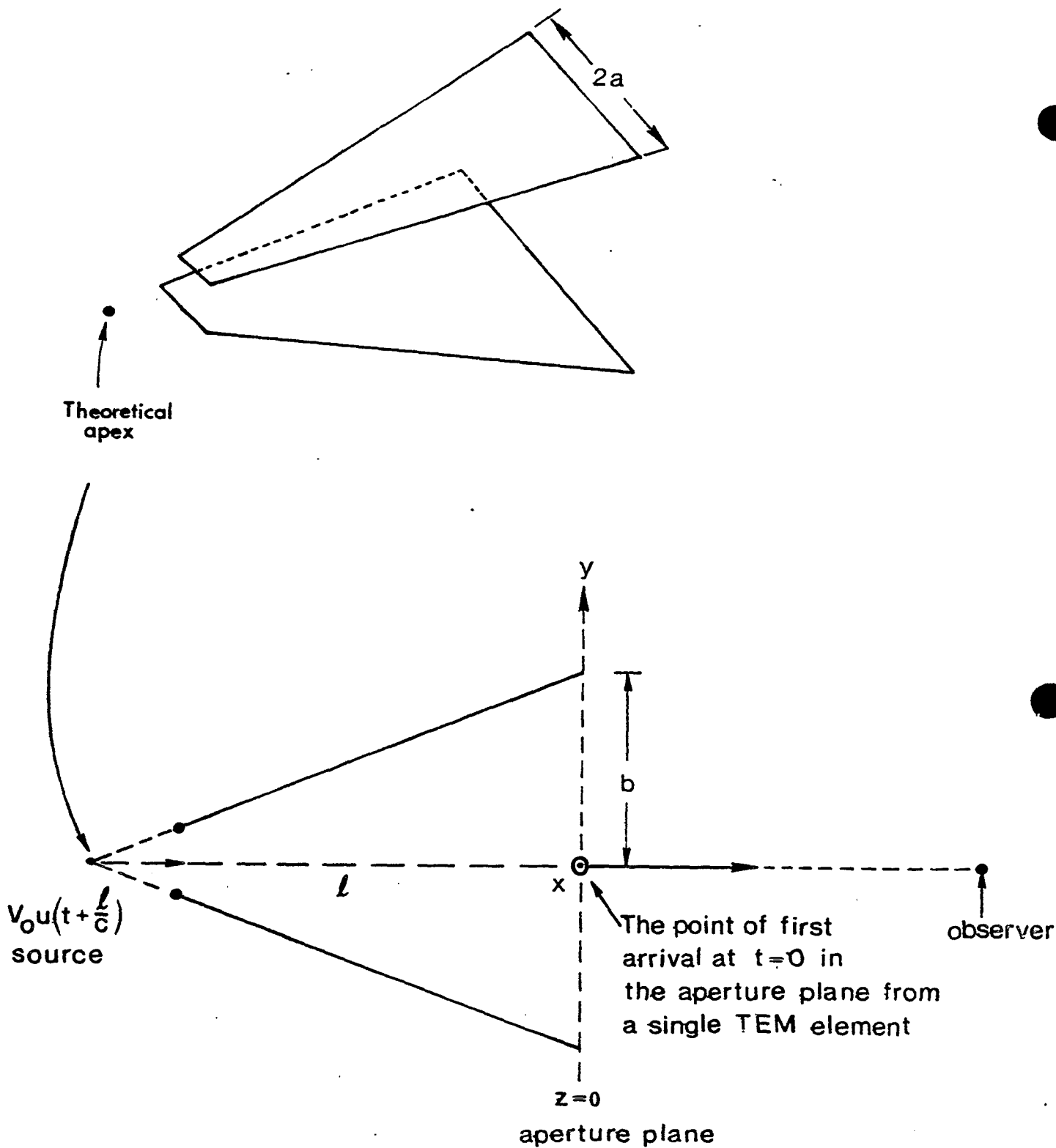
Figure 6. Conical wave launcher and its source point
in the aperture plane z = 0

Comparing $\vec{E}_1(\vec{r},t)$ from (11) with that in (3), it is evident that

$$\vec{F}(\theta = 0, \phi) = \frac{l}{2b} \ \vec{E}_{rel} \tag{12}$$

Using the above result for $| \ \vec{F} \ |$ in (9) we have

$$t_1 = \frac{A}{2\pi c \ (2b)} \left[\frac{l}{2b} E_{y_{rel}}(0,0) \right]^{-1}$$

$$= \frac{4ab}{4\pi cb} \left[\frac{l}{2b} E_{y_{rel}}(0,0) \right]^{-1}$$

$$= \frac{a}{c\pi} \left[\frac{l}{2b} E_{y_{rel}}(0,0) \right]^{-1} \tag{13}$$

or in a normalized sense,

$$\frac{ct_1}{a} = \frac{1}{\pi} \left[\frac{l}{2b} E_{y_{rel}}(0,0) \right]^{-1} \tag{14}$$

The above equations (13) and (14) are useful in estimating an effective rate of rise in the far field, from all the sources, in terms of the normalized field at a single reference point and the geometrical parameters of the unit cell, under the assumption of an infinite planar array. Clearly, many ways of normalizing t_1 are possible to display various dependencies, and for two illustrative geometries of unit cells, these are computed, tabulated and plotted in the appendix at the end of this note.

Recall that the effective rate of rise is dependent on the source point field $E_{y_{rel}}(0,0)$. In the next two sections, we shall briefly review available formulations for obtaining this field, under cylindrical and conical approximations respectively.

V. Fields on Flat-Plate Cylindrical Transmission Line

In estimating the early-time performance of an array of conical launchers, one may treat the launchers as an array of spherical TEM elements which need to be characterized by the field at the source point termed $\vec{E}_{rel}$ in earlier discussions. Now let this vector be in the y direction (by symmetry). Although the launchers are sections of conical transmission lines, the field at the reference point, in cases of long conical lines can be approximated by the field in a cylindrical transmission line whose width and separation are the same as that of the conical line at the aperture plane $z = 0$. If a cylindrical approximation is deemed inadequate, fields in the conical line may be used as reviewed and specialized later. In this section, we consider two possible configurations of the cylindrical transmission line as shown in figures 7 and 8 and review the fields at the reference points indicated in both. This problem has been extensively studied [7, 9, 10 and 11] and we need only to extract the desired result of the electric field at the specialized locations. With reference to the symmetric case of figure 7 $E_{y_{rel}}$ at the origin is given by (equation (B.31) of [11])

$$E_{y_{rel}}(0,0) = \left[\frac{\pi}{2K(m_1)\,E(m)} \right] \tag{15}$$

where K and E are complete elliptic integrals of the first and second kinds of parameter m (or $m_1 = 1-m$) which is obtained as a function of (b/a) via a numerical solution of the appropriate conformal transformation equations. Using (15) in (13), we get

$$t_{1_{cyl}}^{(sym)} = \frac{a}{c\,\pi} \, \frac{2b}{l} \left[\frac{2K(m_1)\,E(m)}{\pi} \right] \tag{16}$$

which can be normalized in any number of different ways, as discussed later in the appendix.

With reference to the asymmetric case of figure 8, the reference point is now located half way up between the top plate and the ground plane (i.e. $x/b = 0$ and $y/b = 0.5$). The relative field $E_{y_{rel}}(0,0.5)$ is available in closed form [11] along the y axis $(x/b = 0)$ as follows

$$E_{y_{rel}}(0,y/b) = \frac{\pi}{2K(m_1)\left[E(m) - m_1 K(m)\,sn^2(u \mid m_1) \right]} \tag{17}$$
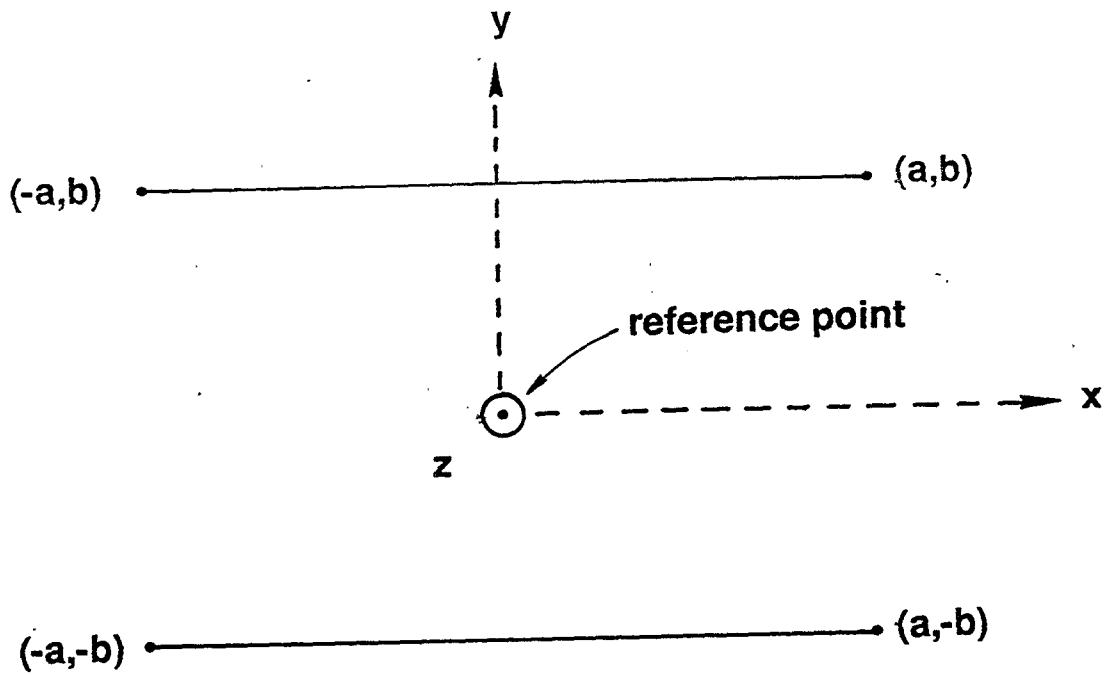
Figure 7. Transverse plane of a symmetrical two-parallel-plate transmission line
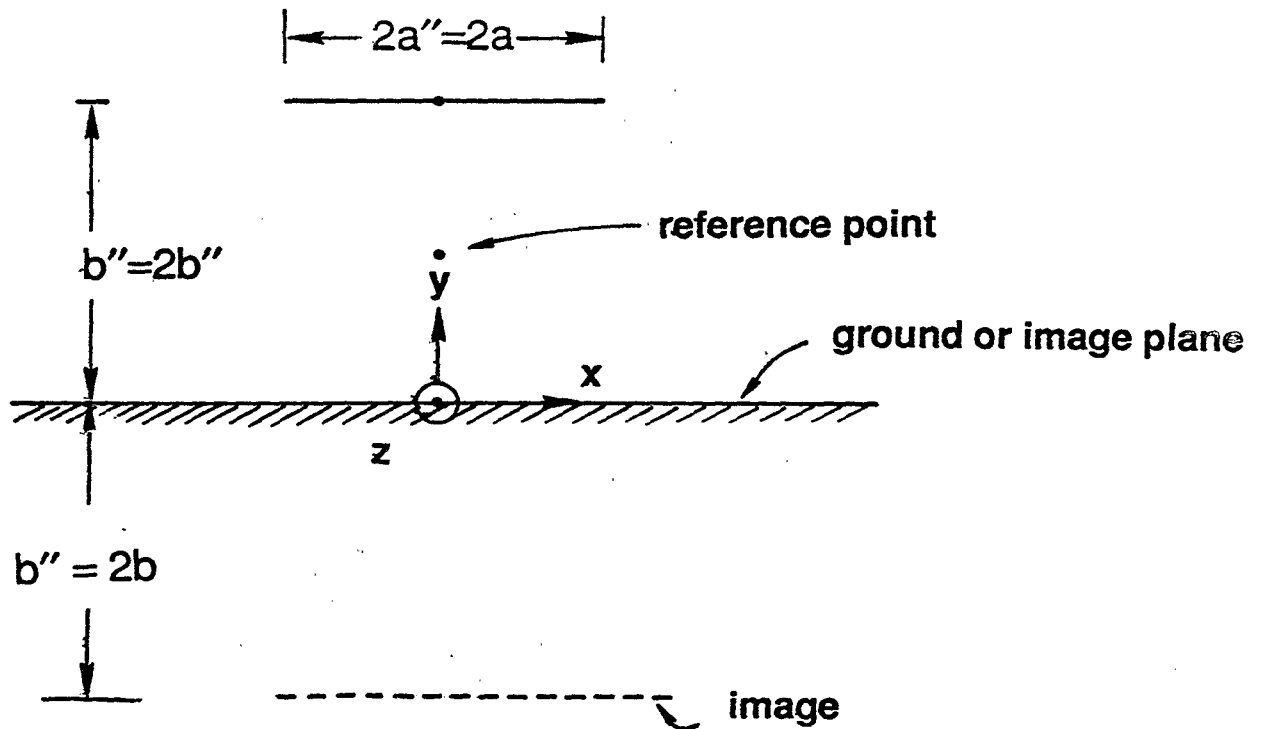
Figure 8. Transverse plane of a transmission line formed by a single plate above and parallel to a ground plane

The above expression is for any point on the y axis and sn is an elliptic function of the argument u which is the (y/b) dependent electric potential. For (y/b) also $= 0$, $u = 0$ and one recovers the origin field. The parameters m, $m_1 = 1-m$ and the potential u are all to be obtained from numerical computations on the conformal transformation equations in many references e.g. [11], as a function of $b''/a'' = (2b/a)$.

Once the field at the reference point is known, the effective rate of rise for this asymmetric case of figure 8 is easily written down using (13) as

$$t_{1_{cyl}}^{(asym)} = \frac{a}{c\pi}\left[\frac{l}{2b}E_{y_{rel}}(0,0.5)\right]^{-1} \qquad (18)$$

We have thus seen that if one makes the cylindrical approximations where the flat plates of the launchers are parallel to each other, the source point fields are known in closed form via conformal transformations, and the far-field rate of rise can be estimated readily. However, more accurate evaluations can be made by using conical-transmission-line-field results as opposed to cylindrical transmission lines. The cylindrical-line fields are reviewed here in this section for completeness and also to verify later that as the length of the conical line is increased, the results should asymptotically approach the cylindrical-line approximation. In the following section, we review the conical-transmission-line fields.

VI. Fields on Flat-Plate Conical Transmission Line

Similar to the cylindrical transmission-line situation, we require the field at the reference point in the transverse plane of a conical transmission line. The conical transmission line can be made up of two flat plates of triangular shapes as in figure 9 or a triangular-shaped top plate placed above a ground plane as shown in figure 10. The impedances [12] and spherical TEM mode fields [13] have been studied in the past. For a TEM mode on a conical transmission line, the wavefront is spherical. The TEM potential and field distributions can be solved through a two-dimensional Laplace equation in the transverse coordinates which can in turn be solved by a combination of stereographic and conformal transformations [7]. The above procedure is well documented in [13] and, reviewed and applied to a practical conical transmission line in [14] and there is no need to reproduce the mathematical formulation here. Suffice it to say that the fields at the reference point are calculable using the procedures developed in [14]. For both cases, the far field is of the form

$$\vec{E}(\vec{r},t) \simeq \frac{V_0}{r}\left[\frac{l}{2b}\vec{E}_{rel}(\text{reference point})\right] u(t-\frac{r}{c}) \qquad (19)$$

For the symmetric conical transmission line of figure 9 the reference point is the origin itself and for the asymmetric case of figure 10, the reference point is exactly half way up between the top plate and the ground plane. For the symmetric case of figure 9, $E_{y_{rel}}(0,0)$ is available in closed form (see equation (4) of [13]) whereas a numerical solution is required for the case of a plate above ground plane with the reference point in between. Rather than repeat the detailed formulae from the quoted references, we only remark that $E_{y_{rel}}$ at reference points are computable as is done later in the appendix.
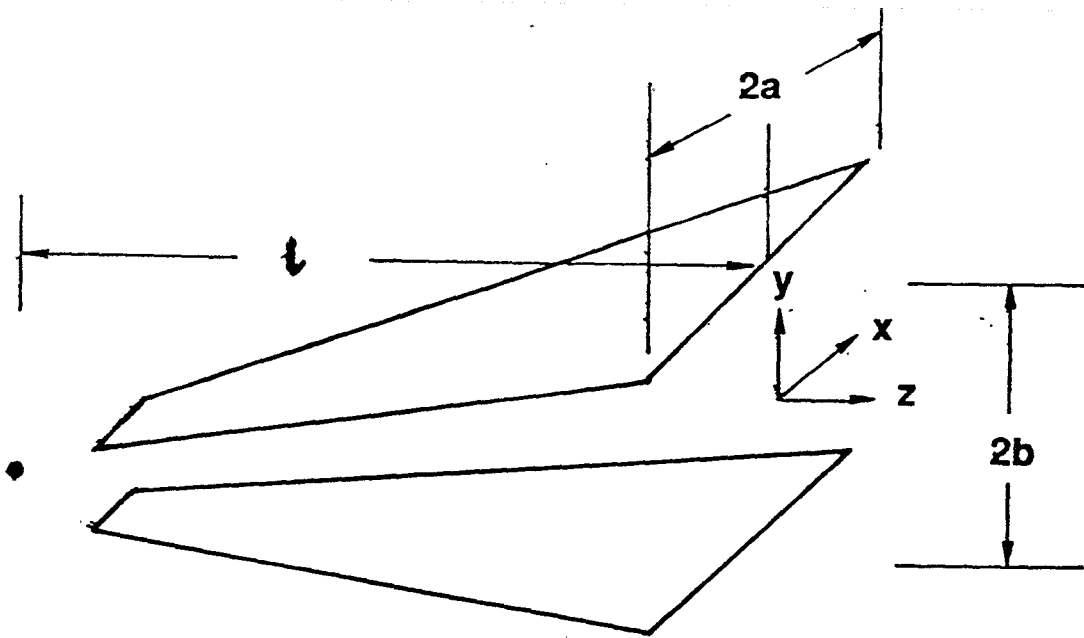
Figure 9. A symmetric flat-plate conical line launcher
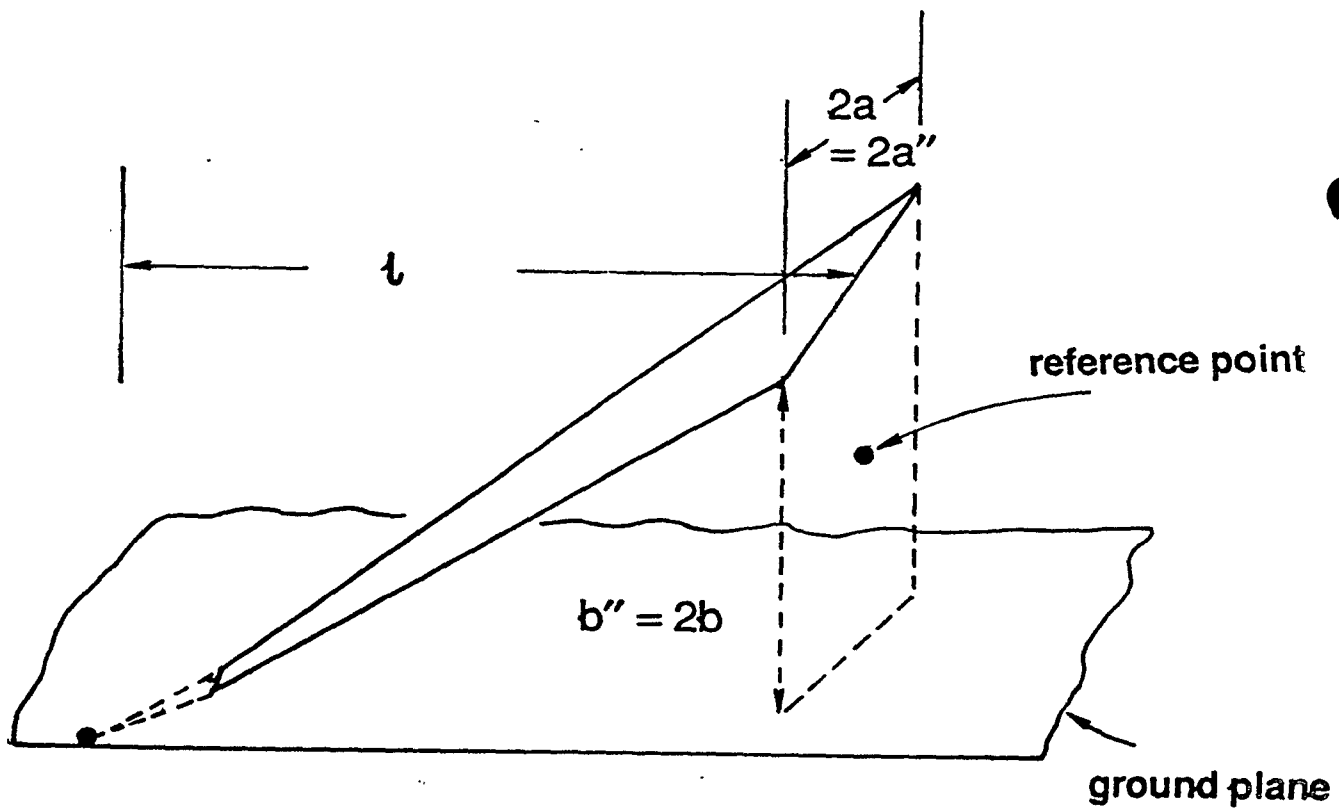
Figure 10. Flat-plate above a ground plane

VII. Early-Time Performance of Arrays of Flat-Plate Conical Transmission Lines

We have seen earlier in Section IV, that the effective rise time can in general be written as

$$t_1 = \frac{A}{2\pi c(h)} (F_y(\theta, \phi))^{-1}$$

$h \equiv$ spacing between spherical TEM elements

in the direction of the electric field at the $\qquad\qquad$ (20)

aperture plane $= 2b$

$$\vec{F} = \frac{l}{2b} \vec{E}_{rel} \text{(reference point)}$$

Let us designate $2b$ and $2a$ to be the spacings along the directions of the electric and magnetic fields respectively at the aperture plane, so that the area of the unit cell is

$$A = 4ab$$

$$t_1 = \frac{a}{c\pi} \left[\frac{l}{2b} E_{y_{rel}} \right]^{-1} \qquad\qquad (21)$$

$$ct_1 = \frac{a}{\pi} \left[\frac{l}{2b} E_{y_{rel}} \right]^{-1}$$

$$\frac{ct_1}{\sqrt{A}} = \frac{a}{\pi\sqrt{A}} \left[\frac{l}{2b} E_{y_{rel}} \right]^{-1}$$

$$= \frac{2ab}{\pi\sqrt{A}} \frac{1}{l} \frac{1}{E_{y_{rel}}}$$

$$= \frac{\sqrt{A}}{l} \frac{1}{2\pi} \frac{1}{E_{y_{rel}}} \qquad\qquad (22)$$

or

$$\frac{ct_1}{\sqrt{A}} \frac{l}{\sqrt{A}} = \frac{1}{2\pi} \frac{1}{E_{y_{rel}}} \tag{23}$$

The normalization of (23) is desirable so that the arbitrariness in the choice of selecting a or b for normalization is removed. Other possibilities are to consider (ct_1/d) for example, where d is either $\sqrt{a^2 + b^2}$ or $\left[\sqrt{l^2 + a^2 + b^2} - l\right]$, which are respectively half the diagonal distance in the unit cell and the dispersion distance [8] over the unit cell in the aperture plane.

Two specific candidate geometries for the unit cell are considered in Appendix A based on discussions or reviews thus far. For these geometries, numerical computations are made to determine normalized rise times. Quantitative results are presented in the appendix.

VIII. Summary

In this note, we have addressed the early-time performance of infinite planar arrays of spherical TEM elements. Earlier works had considered infinite planar biconical arrays and this note has extended such a study to conical wave launcher arrays. It is as though the flat plates of planar bicones have been rotated to form conical-transmission-line wave launchers. Significant improvements can be achieved over the planar bicones by such a modification of the individual elements. Similar to the development of the array factor in antenna array problems, the far field due to all the sources can be expressed in terms of the field from a single element, which in itself is related to the field at a reference point in the aperture of a single element. For an ideal step-function source, an effective rate of rise in the distant field is defined in a manner suitable for computations. Two possible geometrical configurations called the symmetric and asymmetric configurations are identified. Quantitative estimates of the effective rates of rises for both of these cases are made, tabulated and plotted. These tables and plots could serve as design tools for such arrays. They exhibit the improvement derivable from conical-wave-launcher arrays over the performance of planar-biconical arrays. In general, the longer the wave launcher, the better is the performance for times less than the time of mutual interaction effects. In other words, the field at the reference point of one TEM element has a clear time in which it is unaffected by the presence of an adjacent cell's conductors. This clear time depends on the length of the launcher as well as the unit-cell dimensions. So, the lengths of the conical launchers should be sufficiently large to obtain the improvement over the planar biconical case, but not too large to be adversely impacted by the mutual interaction effects. Certain experimental optimization appears to be in order.

APPENDIX-A
Geometry of Arrays of Flat-Plate Conical
Transmission Lines and Numerical Results

The purpose of this appendix is to discuss two possible geometrical configurations forming arrays of flat-plate conical transmission lines. The two geometrical configurations, and the results of numerical evaluations are discussed. The two configurations are termed symmetric and asymmetric. They are described below.

1. Symmetric Configuration

This is a staggered array of conical wave launchers as illustrated via different views in figure A.1. Two triangular shaped flat-plates form a single conical wave launcher.

The reference point in the aperture plane ($z = 0$) is shown in figure A.2 and a single switch in a unit cell at the switch plane ($z = -l_1$) is shown in figure A.3. As is seen in these figures, the plates are $2a$ wide and separated by $2b$ at the aperture plane, while the width and separation are $2a'$ and $2b'$ at the switch plane. It is not essential, but mechanically convenient, to impose the condition $(b'/a') = (b/a)$ resulting in flat plates of triangular shapes. In principle, (b'/a') can be larger, equal to or smaller than (b/a).

We now consider the impedances seen by the sources. As the sources are turned on at the switchplane, it takes some finite time for each cell to be impacted by the presence of the other cells. Consequently, at early times (or high frequencies), the impedance $Z_{early-time}^{(sym)}$ seen by the sources is simply the characteristic impedance of the TEM mode in an infinitely long conical line which may be written as

$$Z_{early-time}^{(sym)} = Z_0 f_{gh} (b'/a')$$ (A.1)

$$Z_0 = \sqrt{\mu_0/\varepsilon_0} \equiv \text{characteristic impedance of free space}$$

As time progresses, the mutual interactions between cells occur, resulting at late times, in the launching of spherical TEM waves in both + and $-z$ directions. The late time (or low-frequency) impedance $Z_{late-time}^{(sym)}$ can then be written as

$$Z_{late-time}^{(sym)} = \frac{1}{2} Z_0 \left[\frac{b}{a} \right]$$ (A.2)

a) Front view

b) Back view

c) Side view
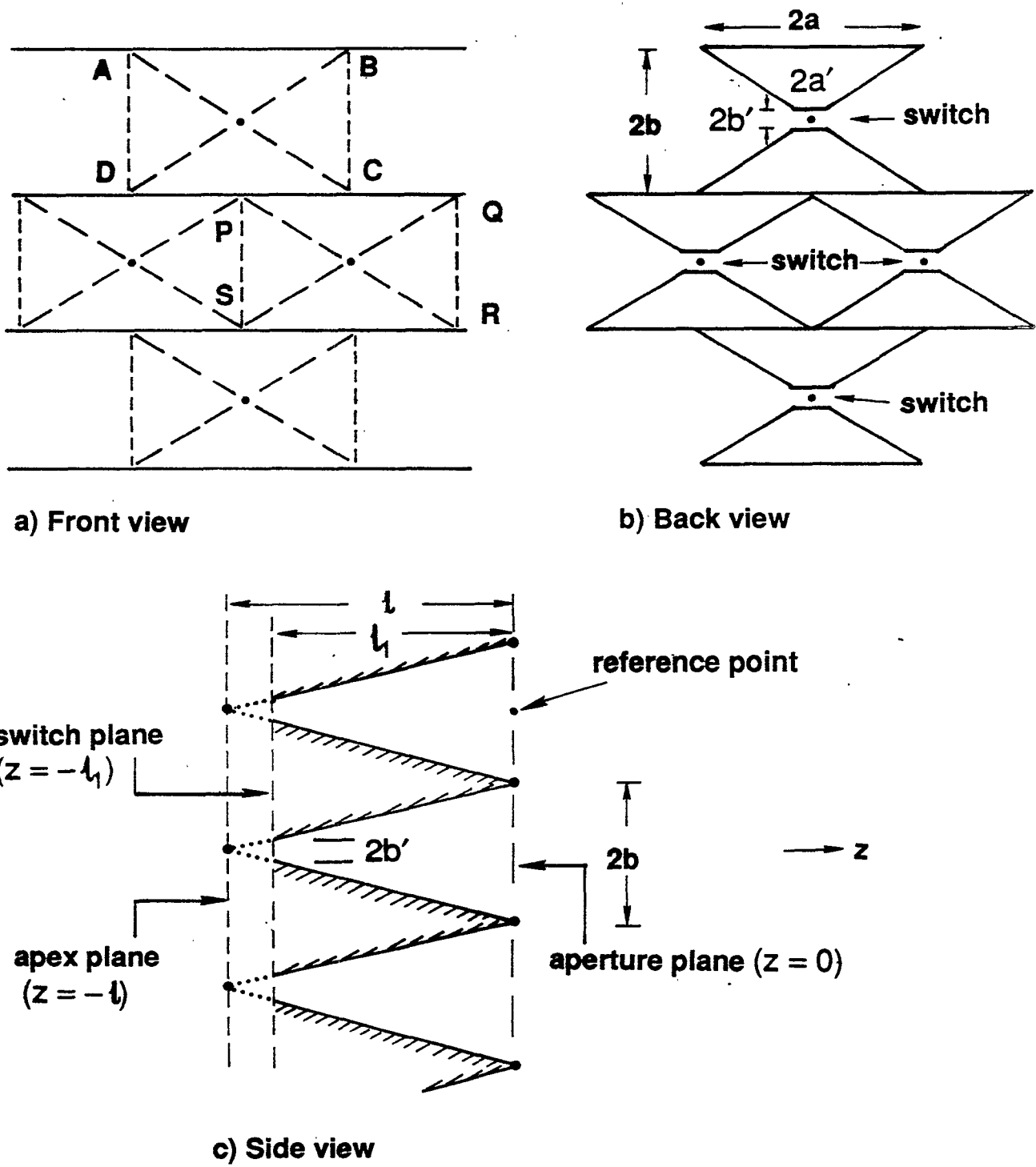
Figure A.1   Staggered array of flat-plate conical launchers in a symmetric configuration
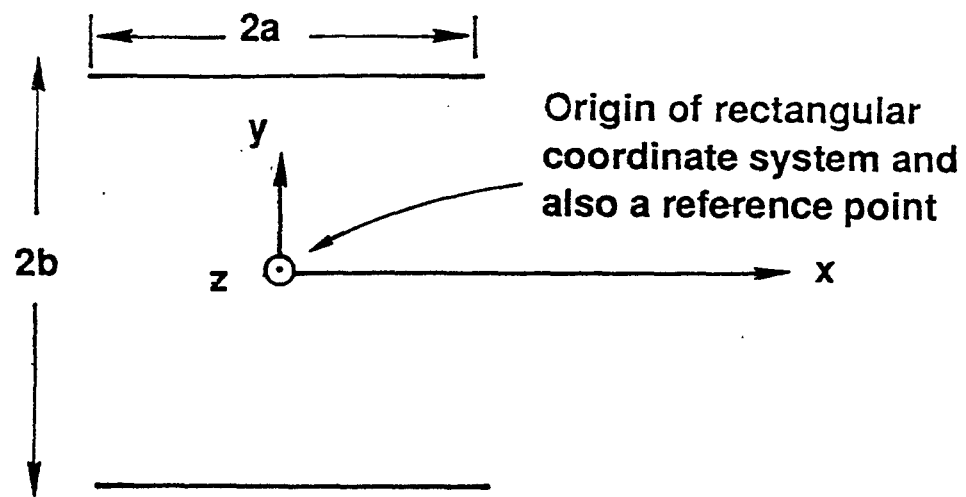
Figures A.2 Reference point in the aperture plane
$z = 0$, for symmetric configuration

switch closure at $z = -\dfrac{\ell_1}{c}$
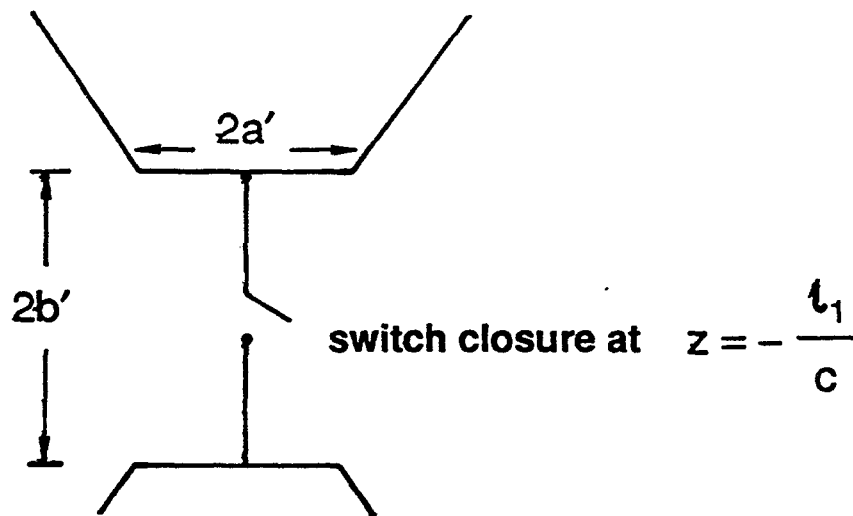
Figure A.3. Gecmetry of the unit cell at the switch
plane $z = -\ell_1$, for the symmetric configuration

In the above expression the factor of (1/2) accounts for the presence of waves in both forward and backward directions.

It is desirable to require the same early and late time impedances leading to

$$\frac{1}{2} \frac{b}{a} = f_{gh}(b'/a')$$ (A.3)

so as to minimize reflection magnitudes back to the switches.

Furthermore, it may be mechanically convenient to choose $(b'/a') = (b/a)$ so that the wave launchers may be made from triangular shaped plates. For this special case, by interpolating the tabulated results in [10], we have

$$\frac{1}{2} \frac{b}{a} = f_{gh}(b'/a') = f_g(b/a)$$

$$(b/a) = (b'/a') = 0.877$$ (A.4)

$$f_{gh} = 0.438$$

$$Z^{(sym)}_{early-time} = Z^{(sym)}_{late-time} = 165\Omega$$ (A.5)

For obtaining the impedances, we have implicitly used a parallel-plate or cylindrical approximation, which is adequate for $l/b \geq 3$. The above value of $(b/a) = 0.877$ is mechanically convenient, and seen to have desirable impedance properties and hence is an interesting special case. It is considered useful to parametrically vary (b/a) and the length of the launcher.

Before setting up the normalizations for the effective rate of rise in the far field, it is also important to distinguish between the aperture plane that contains the open end of all launchers, the apex plane that contains the theoretical apices of all the launchers, and the switch plane near the apex plane that contains the switches whose electrodes are electrically connected to the launcher plates. These three planes are indicated in figure A.1c. The individual switches, because of their sizes, however small, cannot be placed at the apices and a minimum separation between the plates is essential for high-voltage standoff.

Returning to the discussion of rate of rise, we have seen earlier in (13)

$$t_1 = \frac{a}{c\pi} \frac{2b}{l} \frac{1}{E_{y_{rel}}}$$ (A.6)

-25-

where $E_{y_{rel}}$ is the field at a reference point which is shown in figures A.1c and A.2. For numerical purposes of computing, tabulating and plotting, the following normalizations are employed

$$\frac{ct_1}{\sqrt{A}} = \frac{ct_1}{\sqrt{4ab}}$$

$$= \frac{2ab}{\pi l \sqrt{4ab}} \frac{1}{E_{y_{rel}}} = \frac{\sqrt{A}}{l} \frac{1}{2\pi} \frac{1}{E_{y_{rel}}} \tag{A.7}$$

or

$$T_{n1}^{(sym)} = \left[\frac{ct_1}{\sqrt{A}} \right] = \frac{\sqrt{A}}{l} \frac{1}{2\pi} \frac{1}{E_{y_{rel}}(0,0)} \tag{A.8}$$

and

$$T_{n2}^{(sym)} = \left[\frac{ct_1}{\sqrt{A}} \frac{l}{\sqrt{A}} \right] = \frac{1}{2\pi} \frac{1}{E_{y_{rel}}(0,0)} \tag{A.9}$$

The above two normalized effective times are computed, tabulated and plotted. Before the numerical results are presented, we discuss the case of planar bicones (i.e. $l = 0$) for base-line comparison. A unit cell of the symmetric configuration of the planar biconical launchers is shown in figure A.4. The half angle ψ of the planar bicones is given by

$$\psi = arctan(a'/b') \tag{A.10}$$

It is also noted that $(a/b) = (a'/b')$ if and only if the half angle $\psi = (\pi/4)$. Also, since $l = 0$ for the planar case, the normalization of (A.9) is unsuitable and we use the normalization implied by (A.8) as follows

$$T_{n1}^{(sym-planar)} = \frac{ct_1}{\sqrt{A}} \tag{A.11}$$

which can be evaluated as follows. For each value of (b/a), the equal impedance criterion of (A.3) gives us a value of (b'/a') and implicitly ψ via (A.10). Tables 1 and 2
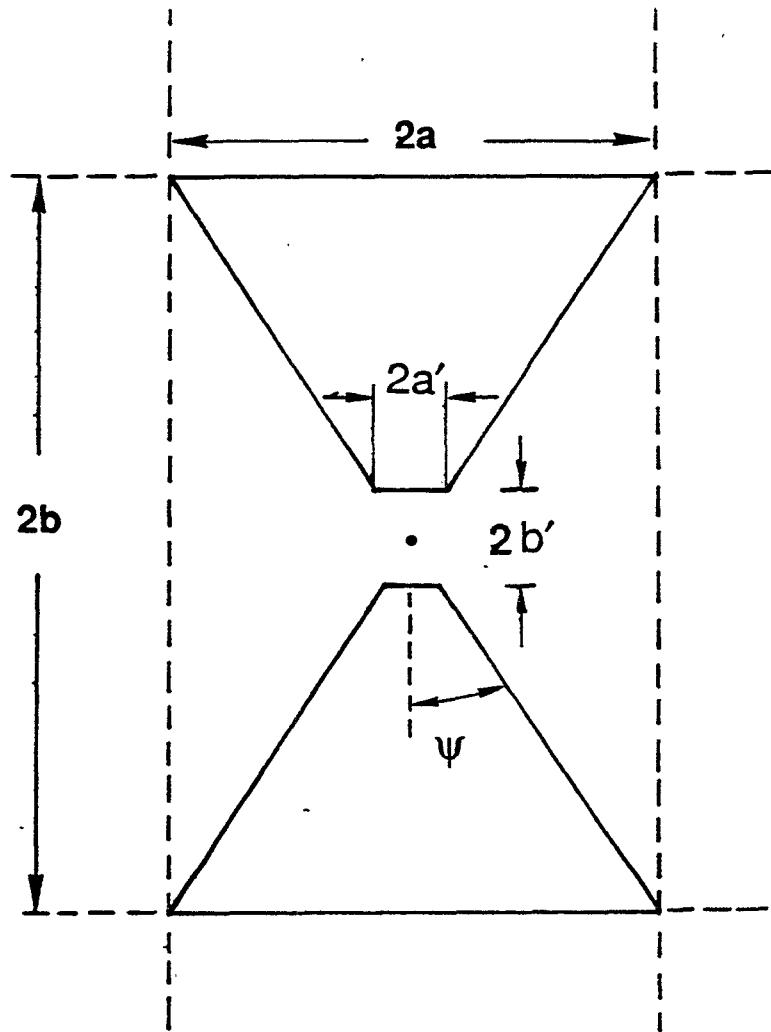
Figure A.4. Unit cell of planar biconical launchers in a symmetric configuration $(\ell/\sqrt{A}) = 0$.

in [1] lead to the value of (ct_1/a), noting that the symbol b in [1] is the same as a in this note. Once (ct_1/a) is known from Table 2 of [1], we can get

$$T_{n1}^{(sym-planar)} = \left[\frac{ct_1}{a}\right]\frac{a}{\sqrt{A}} = \left[\frac{ct_1}{a}\right]\frac{1}{2\sqrt{b/a}}$$

$$\text{for} \quad l/\sqrt{A} = 0 \tag{A.12}$$

The result of the above procedure is tabulated in Table 1, for later plotting. Observe the special case of $(b/a) = (b'/a') = 1$ for the planar bicones.

Next, four values of $l/\sqrt{A}$ are considered for the symmetric configuration of figure A.1. They are $l/\sqrt{A} = 1, 2, 5$ and 10. For each $l/\sqrt{A}$, $T_{n1}^{(sym)}$ and $T_{n2}^{(sym)}$ are computed using (A.8), (A.9) as functions of (b/a). The results of these computations are presented in Tables 2a and 2b. Also listed in the Tables 2a and 2b, are the values of (b'/a') and $f_{gh}(b'/a')$. This geometric factor is indicative of the same load impedance seen by the source modules, both at high and low frequencies.

For the symmetric configuration under discussion, we finally consider the case of $l/\sqrt{A} = \infty$. This corresponds to semi-infinitely long wave launchers extending from $z = -\infty$ to the aperture plane at $z = 0$. We have seen earlier in (16), the effective rate of rise is inversely proportional to l so that the normalization of (A.8) is unsuitable and we may use the normalization of (A.9) leading to

$$T_{n1_{cyl}}^{(sym)} = \left[\frac{ct_{1_{cyl}}^{(sym)}}{\sqrt{A}}\right]\frac{l}{\sqrt{A}}$$

$$= \frac{1}{2\pi}\left[\frac{2K(m_1)E(m)}{\pi}\right] ; \quad \text{for} \quad \left[l/\sqrt{A}\right] = \infty \tag{A.13}$$

In the above expression, $m_1 (= 1-m)$ and m are dependent on (b/a) via the familiar conformal transformation equations [7, 9, 10 and 11]. The results for $l/\sqrt{A} = \infty$ are presented in table 3. The special case of $(b/a) = 0.877$ satisfies the equal high and low frequency impedances, while permitting $(b/a) = (b'/a')$, which could be of help in the

$$(l / \sqrt{A}) = 0 \qquad \text{SYMMETRIC}$$

$\dfrac{b}{a}$	$f_{gh}(b'/a')$ $= \dfrac{1}{2}\dfrac{b}{a}$	$\dfrac{2\psi}{\pi}$	ψ	$\dfrac{b'}{a'}$	$\dfrac{ct_1}{a}$	$T_{n1}^{(sym-planar)}$ $= \dfrac{ct_1}{\sqrt{A}}$
0.000	0.000	1.000	$0.500\,\pi$	0.000	1	∞
0.500	0.250	0.890	$0.445\,\pi$	0.175	1.008	0.713
0.877	0.438	0.590	$0.295\,\pi$	0.751	1.115	0.595
*1.000	0.500	0.500	$0.250\,\pi$	1.000	1.180	0.590
1.500	0.750	0.235	$0.118\,\pi$	2.585	1.562	0.638
2.000	1.000	0.110	$0.055\,\pi$	5.730	2.014	0.712
3.520	1.760	0.010	$0.005\,\pi$	63.657	3.527	0.940

* Special case of $(b/a) = (b'/a') = 1$ and
equal low and high frequency impedances.

Table 1. Normalized effective rate of rise for planar bicones
$(l/\sqrt{A}) = 0$, in a symmetric configuration.

$\dfrac{b}{a}$	f_g *	$\dfrac{b'}{a'}$ (using (A.3))	$l/\sqrt{A} = 1$		$l/\sqrt{A} = 2$	
			$T_{n1}^{(sym)}$	$T_{n2}^{(sym)}$	$T_{n1}^{(sym)}$	$T_{n2}^{(sym)}$
0.230	0.115	0.141	0.1562	0.1562	0.0791	0.1583
0.270	0.135	0.171	0.1557	0.1557	0.0791	0.1583
0.320	0.160	0.210	0.1550	0.1550	0.0790	0.1580
0.370	0.185	0.251	0.1546	0.1546	0.0790	0.1581
0.430	0.215	0.308	0.1538	0.1538	0.0790	0.2580
0.510	0.255	0.388	0.1535	0.1535	0.0789	0.1577
0.590	0.295	0.475	0.1530	0.1530	0.0789	0.1578
0.690	0.345	0.598	0.1525	0.1525	0.0791	0.1582
0.810	0.405	0.770	0.1526	0.1526	0.0797	0.1595
0.950	0.475	1.010	0.1538	0.1538	0.0804	0.1608
1.100	0.550	1.299	0.1548	0.1548	0.0818	0.1636
1.290	0.645	1.896	0.1572	0.1572	0.0834	0.1667
2.060	1.030	6.356	0.1649	0.1649	0.0856	0.1713
3.280	1.640	43.197	0.1629	0.1629	0.0880	0.1759
3.830	1.915	102.481	0.1767	0.1767	0.0913	0.1827
4.470	2.235	280.047	0.1923	0.1923	0.0947	0.1894
7.130	3.565	18.27×10^3	0.2019	0.2019	0.0985	0.1971
8.330	4.165	0.12×10^6	0.2035	0.2035	0.1024	0.2048
9.720	4.860	1.07×10^6	0.2048	0.2048	0.1062	0.2123
11.360	5.680	14×10^6	0.2047	0.2047	0.1104	0.2208

*   High and low frequency impedance normalized to Z_0.

Table 2a.   Normalized effective rate of rise for non-planar conical wave launchers in a staggered symmetric configuration; $l/\sqrt{A} = 1$ and 2

$\dfrac{b}{a}$	f_g *	$\dfrac{b'}{a'}$ (using (A.3))	$l/\sqrt{A} = 5$		$l/\sqrt{A} = 10$	
			$T_{n1}^{(sym)}$	$T_{n2}^{(sym)}$	$T_{n1}^{(sym)}$	$T_{n2}^{(sym)}$
1.51	0.755	2.679	0.0349	0.1749	0.0175	0.1749
1.76	0.880	3.968	0.0361	0.1808	0.0180	0.1808
2.06	1.030	6.356	0.0375	0.1875	0.0187	0.1875
2.40	1.200	10.843	0.0390	0.1954	0.0195	0.1954
2.81	1.405	20.646	0.0408	0.2040	0.0204	0.2040
3.28	1.640	43.197	0.0426	0.2131	0.0213	0.2131
3.83	1.915	102.481	0.0446	0.2229	0.0223	0.2229
4.47	2.235	280.047	0.0466	0.2331	0.0235	0.2351
5.22	2.610	909.614	0.0487	0.2437	0.0245	0.2458
6.10	3.050	3.62×10^3	0.0508	0.2541	0.0257	0.2570
7.13	3.560	18.27×10^3	0.0530	0.2650	0.0268	0.2682
8.33	4.165	0.12×10^6	0.0551	0.2758	0.0279	0.2796
9.72	4.860	1.07×10^6	0.0573	0.2864	0.0291	0.2910
11.36	5.680	14×10^6	0.0594	0.2970	0.0302	0.3026
13.27	6.635	282×10^6	0.0615	0.3077	0.0314	0.3144
15.50	7.750	9.36×10^9	0.0634	0.3173	0.0326	0.3260
18.10	9.050	0.55×10^{12}	0.0654	0.3271	0.0337	0.3375
21.15	10.575	6.69×10^{13}	0.0667	0.3338	0.0349	0.3491
24.70	12.350	1.77×10^{16}	0.0690	0.3453	0.0360	0.3600
28.85	14.425	1.19×10^{19}	0.0708	0.3539	0.0371	0.3712

* High and low frequency impedance normalized to Z^0.

Table 2b.   Normalized effective rate of rise for non-planar conical wave launchers in a staggered symmetric configuration; $l/\sqrt{A} = 5$ and 10

$$(l / \sqrt{A}) = \infty \quad \text{SYMMETRIC}$$

$\dfrac{b}{a}$	m	f_{gh}	$T_{n1_{cyl}}^{(sym)} = \left[\dfrac{ct_1^{(sym)}}{\sqrt{A}} \right] \dfrac{l}{\sqrt{A}}$
0.200	0.99999	0.15407	0.159
0.319	0.99998	0.22182	0.159
0.508	0.99936	0.30976	0.159
0.693	0.99592	0.37969	0.161
0.809	0.99135	0.41781	0.162
0.877	0.99236	0.43850	0.163
0.946	0.98338	0.45784	0.164
1.290	0.95211	0.54285	0.271
1.760	0.89411	0.63305	0.317
2.402	0.80871	0.72679	0.197
3.277	0.70354	0.82275	0.215
4.472	0.59041	0.92001	0.236
6.102	0.48046	1.0180	0.258
8.325	0.38131	1.1164	0.281
11.356	0.29673	1.2151	0.305
15.499	0.22743	1.3139	0.329
21.147	0.17232	1.4127	0.354
28.854	0.12944	1.5116	0.378
45.986	0.08330	1.6599	0.415
73.291	0.05311	1.8082	0.452
100.000	0.03920	1.9072	0.477

*   Special case of $(b/a) = (b'/a') = 0.877$ and

Z (*high frequencies*) $= Z$ (*low frequencies*).

Table 3.   Normalized effective rate of rise for semi-infinitely long launchers $(l/\sqrt{A}) = \infty$, in a symmetric configuration.

actual fabrication of the wave launchers from triangular shaped flat-plate conductors.

The calculated results presented in Tables 1, 2 and 3 are shown plotted in figure A.5. $T_{n1}^{(sym)}$ plotted in the top half of this figure demonstrates the improvement obtainable from non-planar launchers, as compared with the planar biconical launchers. $T_{n2}^{(sym)}$ plotted in the bottom half, shows that as $(l/\sqrt{A})$ is increased, asymptotically the result of the cylindrical transmission line launchers $(l/\sqrt{A}) = \infty$, is approached. In addition, the special cases of (b/a) equalling (b'/a') while satisfying identical high and low frequency impedances are indicated in the plots.

Next, we turn our attention to the computations for the asymptotic configuration of wave launchers.

2. Asymmetric Configuration

This is also a staggered array conical launchers with alternating pairs of continuous and discrete launchers. The continuous conductor is a solid surface in a wedge shape and the discrete ones are triangular shaped flat plates. The array configuration is illustrated in figure A.6 by showing the back, front and side views. The reference point in the aperture plane $z = 0$ is shown in figure A.7 and a single switch in a unit cell at the switch plane is shown in figure A.8.

Once again, as in the symmetric configuration, at early times (or high frequencies), with reference to figure A.8, we have an impedance given by

$$Z_{early-time}^{(asym)} = Z_0 \frac{1}{2} f_{gh} (b''/a'') \tag{A.14}$$

As in figure 8, we compute f_{gh} based on an image behind the ground plane allowing for the factor of $(1/2)$ to relate this impedance to the asymmetric case. Furthermore the argument is (b''/a'') with dimensions at the switch plane as in figure A.8.

As before, after the mutual interactions between cells have occurred, the late-time (or low frequency) impedance is given by

$$Z_{late-time}^{(asym)} = \frac{1}{2} Z_0 (b/a) \tag{A.15}$$

Once again it is desirable to minimize reflection magnitudes back to sources by requiring equal early and late time impedances leading to
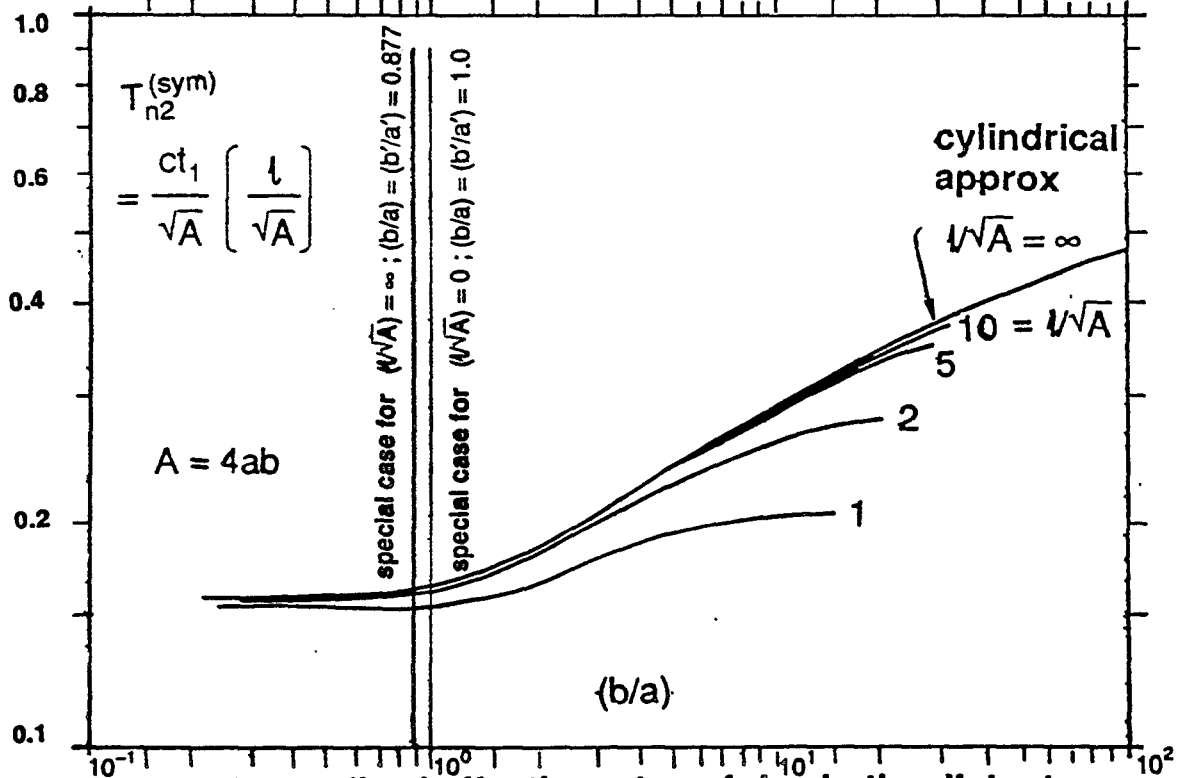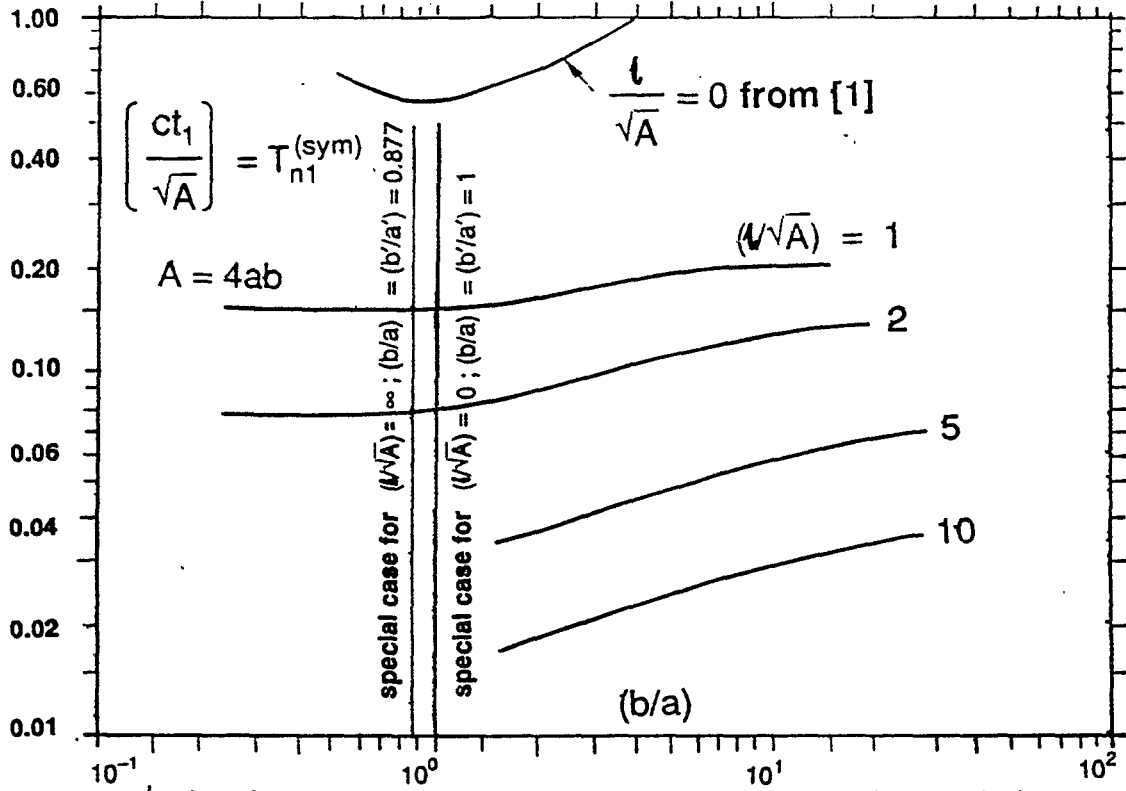
Figure A.5. Normalized effective rates of rise in the distant field along the normal direction for the symmetric configuration
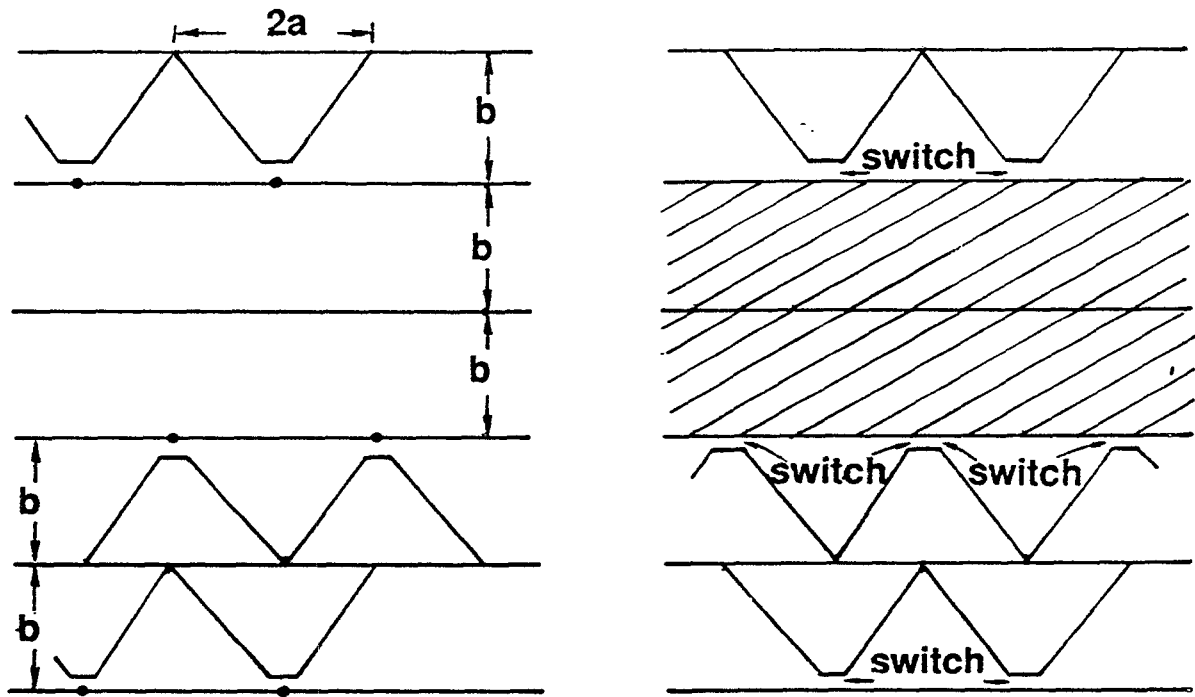
a) Front view

b) Back view
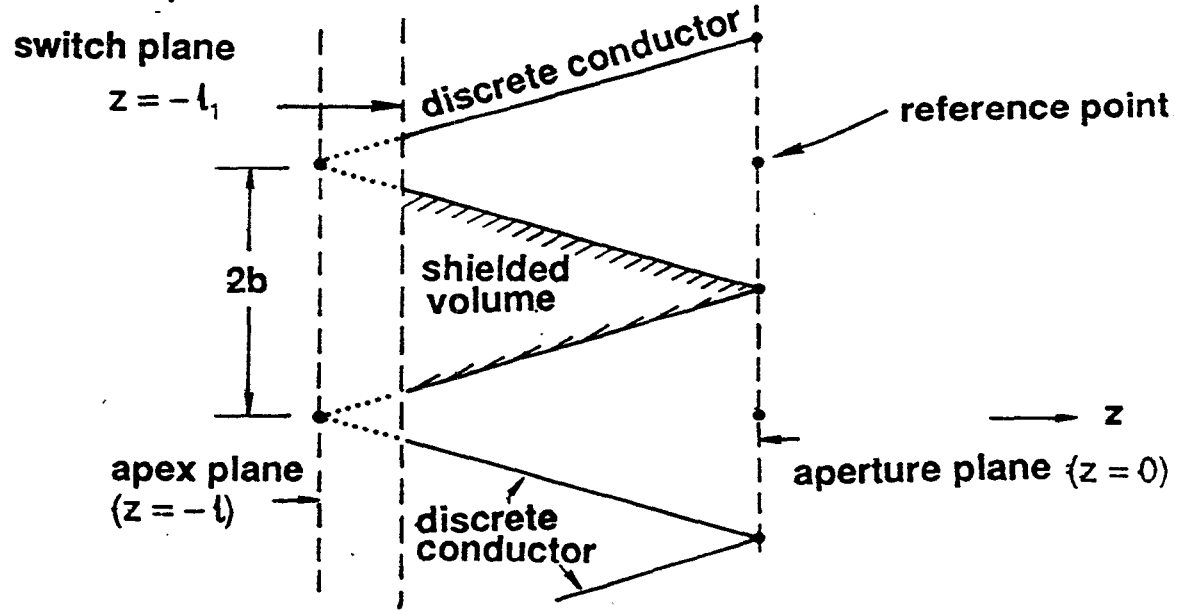
c) Side view

Figure A.6. Staggered array of flat-plate conical
launchers in an asymmetric configuration
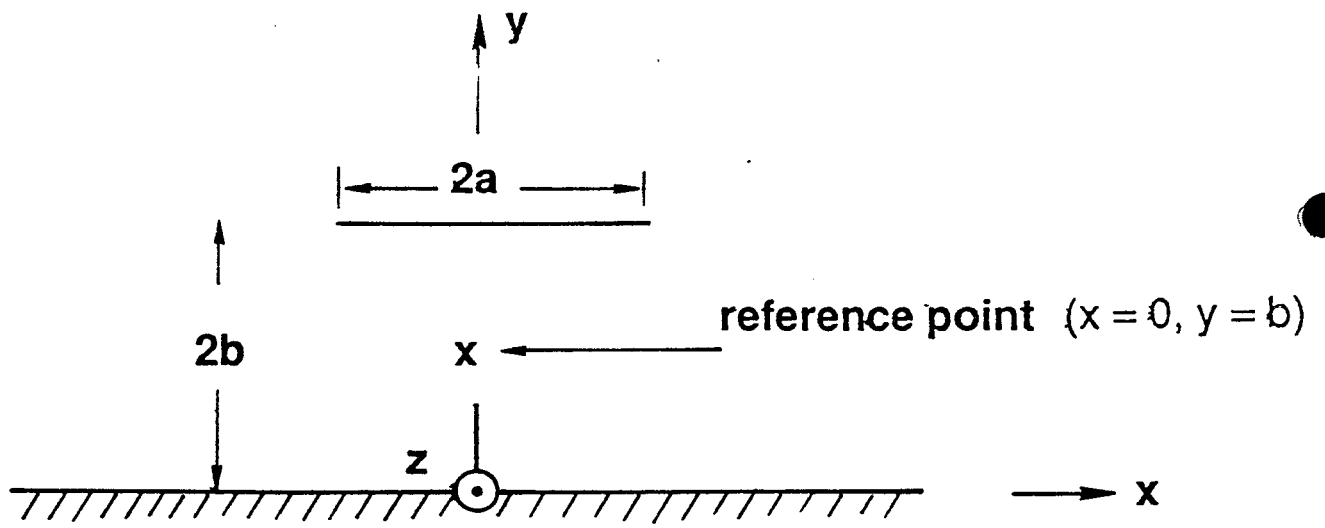
Figure A.7. Reference point in the aperture plane $z = 0$
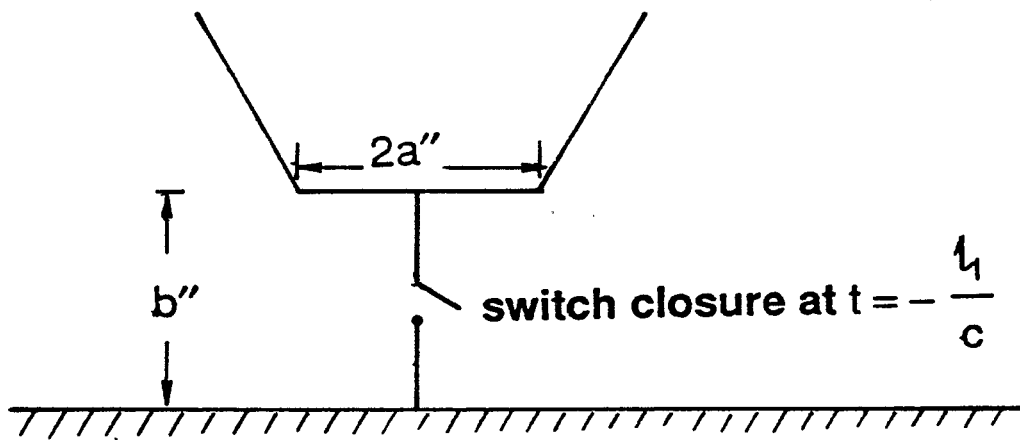
Figures A.8. Geometry of the unit cell at the switch plane $z = -\ell_1$

$$\frac{1}{2} Z_0 \ (b/a) = \frac{Z_0}{2} f_{gh} \ (b''/a'')$$

$$(b/a) = f_{gh}(b''/a'') \qquad\qquad \text{(A.16)}$$

Furthermore, for mechanical convenience if we choose $(2b/a) = (b''/a'')$ so as to make the launchers from triangular plates, we have

$$(b/a) \approx 0.438$$

$$Z_{early-time}^{(asym)} = Z_{late-time}^{(asym)} \approx 82\Omega \qquad \text{for } l/\sqrt{A} = \infty \qquad\qquad \text{(A.17)}$$

Yet another advantage of the asymmetric configuration is the presence of a shielded volume indicated in figure A.6b, which could be useful in shielding trigger electronics, cables from the launching region, etc.

Next, in order to estimate the effective rate of rise in the far field of the asymmetric configuration, we require the field at the reference point in the aperture plane of a unit cell.

This reference point is half way between the plate and the ground plane, as shown in figure A.7 leading to

$$t_1 = \frac{a}{c\pi} \ \frac{2b}{l} \ \frac{1}{E_{y_{rel}}(0, 0.5)} \qquad\qquad \text{(A.18)}$$

With the normalizations as before

$$T_{n1}^{(asym)} = \left[\frac{ct_1}{\sqrt{A}}\right] = \frac{\sqrt{A}}{l} \ \frac{1}{2\pi E_{y_{rel}}} \qquad\qquad \text{(A.19)}$$

$$T_{n2}^{(asym)} = \left[\frac{ct_1}{\sqrt{A}}\right] \frac{l}{\sqrt{A}} = \frac{1}{2\pi E_{y_{rel}}} \qquad\qquad \text{(A.20)}$$

We have computed the above normalized quantities for $(l/\sqrt{A}) = 0, 1, 2, 5, 10$ and ∞, as before, as functions of (b/a). Before we present the results, the planar case of $l/\sqrt{A}$ merits some discussion. A unit cell of the planar biconical launchers in an asymmetric configuration is shown in figure A.9. The half angle ψ is now given by

$$\psi = arctan\ (a''/b'') \qquad\qquad (A.21)$$

For this planar case of $(l/\sqrt{A}) = 0$, each value of (b/a) implies a value of (b''/a'') and ψ via (A.16) and (A.21) and for this value of ψ, (ct_1/a) can be read from Table 2 in [1] as before. The normalized rate of rise $T_{n1}^{(asym-planar)}$ is then given by

$$T_{n1}^{(asym-planar)}\ =\ \frac{ct_1}{\sqrt{A}}\ =\ \frac{ct_1}{a}\ \frac{a}{\sqrt{A}}\ =\ \left[\frac{ct_1}{a}\right]\ \frac{1}{2}\left[\frac{b}{a}\right]^{-1/2}$$

$$\text{for}\ \ l/\sqrt{A}\ =\ 0 \qquad\qquad (A.22)$$

The combination of stereographic projection and conformal transformation for conical transmission lines [12 and 13] is applicable even for the planar case as l becomes zero, resulting in two planar conical plates. Once again, the normalization of $T_{n1}^{(asym)}$ is used and $T_{n2}^{(asym)}$ is inappropriate as l becomes zero. The results for the planar case are presented in Table 4. The results for finite $l/\sqrt{A}$ values of 1, 2, 5 and 10 are presented in Tables 5a and 5b, and the results for the case of $l/\sqrt{A} = \infty$ can be interpreted from the earlier results in Table 3 for the symmetric case. The special case of $(2b/a) = (b''/a'')$ for $l/\sqrt{A} = \infty$ is also indicated. Recall that (b''/a'') is computed by requiring that the early-time (or high-frequency) impedance be the same as late-time (or low-frequency) impedance. The special case of $(2b/a) = 0.877$ or $(b/a) = 0.438$ simply offers an added mechanical advantage. The results of the asymmetric configuration are plotted in figure A.10. It is observed that the length has appreciable effect on the rate of rise and the cylindrical case of a semi-infinitely long launcher is approached asymptotically.
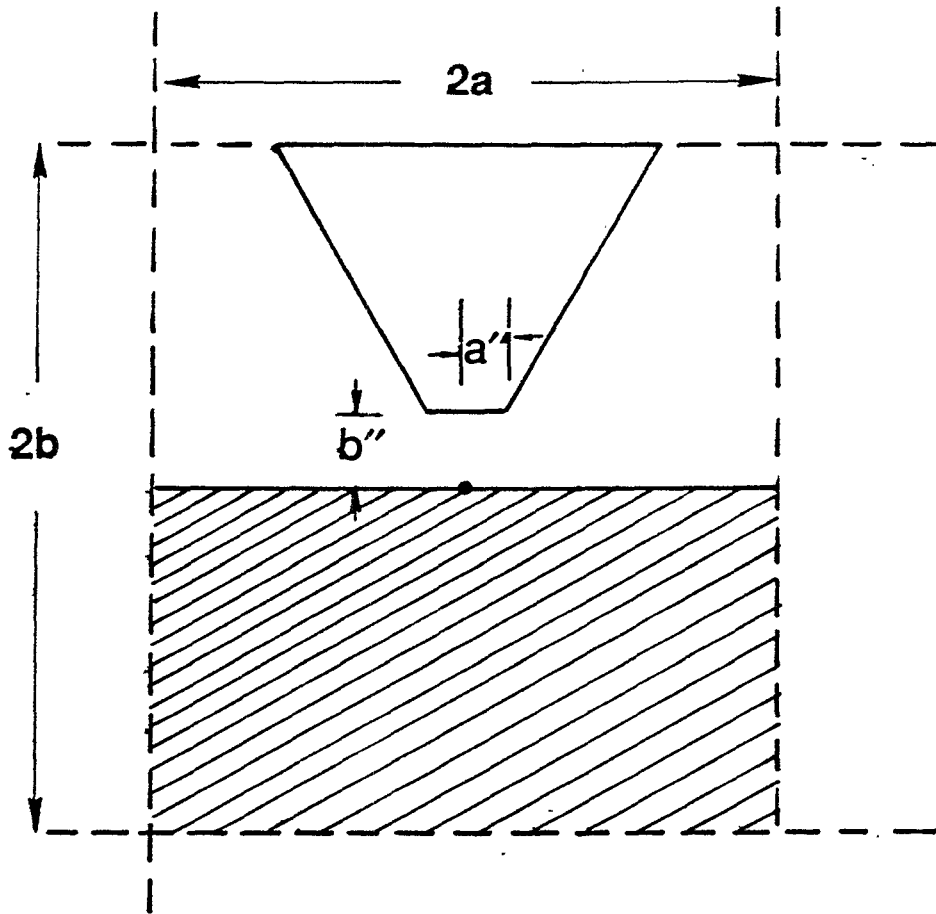
Figure A.9. Unit cell of planar biconical launchers in an asymmetric configuration $(l/\sqrt{A}) = 0$.

$$(l / \sqrt{A}) \quad = \quad 0 \qquad \text{ASYMMETRIC}$$

$\dfrac{b}{a}$	$f_{gh}(b''/a'')$ $=\dfrac{b}{a}$	$\dfrac{2}{\pi}\psi$	ψ	$\dfrac{b''}{a''}$	$\dfrac{ct_1}{a}$	$T_{n1}^{(asym-planar)}$ $=\dfrac{ct_1}{\sqrt{A}}$
0.000	0.000	1.000	$0.500\,\pi$	0.000	1.00000	∞
0.200	0.200	0.950	$0.475\,\pi$	0.079	1.00154	1.120
0.300	0.300	0.815	$0.408\,\pi$	0.299	1.02154	0.933
0.500	0.500	0.500	$0.250\,\pi$	1.000	1.18034	0.835
1.000	1.000	0.110	$0.055\,\pi$	5.730	2.01368	1.007
1.413	1.413	0.030	$0.015\,\pi$	21.20	2.82885	1.190
2.055	2.055	0.004	$0.002\,\pi$	159.1	N/A	N/A
2.496	2.496	0.001	$0.0005\,\pi$	636.6	N/A	N/A

(* marks the 0.500 row)

N/A: (ct_1/a) is not available for such low ψ values in Table 2 of [1].

* Special case of $2(b/a)=(b''/a'')$ and equal low and high frequency impedances.

Table 4. Normalized effective rate of rise for planar asymmetric configuration $(l/\sqrt{A})=0$.

$\dfrac{b}{a}$	f_g *	$\dfrac{b''}{a''}$ (using (A.16))	$l/\sqrt{A} = l$		$l/\sqrt{A} = 2$	
			$T_{n1}^{(asym)}$	$T_{n2}^{(asym)}$	$T_{n1}^{(asym)}$	$T_{n2}^{(asym)}$
0.230	0.230	0.338	0.1579	0.1579	0.0794	0.1588
0.270	0.270	0.418	0.1577	0.1577	0.0794	0.1588
0.320	0.320	0.535	0.1573	0.1573	0.0793	0.1586
0.370	0.370	0.666	0.1573	0.1573	0.0793	0.1587
0.430	0.430	0.850	0.1567	0.1567	0.0793	0.1586
0.510	0.510	1.15	0.1567	0.1567	0.0792	0.1584
0.590	0.590	1.52	0.1563	0.1563	0.0791	0.1582
0.690	0.690	2.18	0.1554	0.1554	0.0790	0.1580
0.810	0.810	3.18	0.1548	0.1548	0.0791	0.1582
0.950	0.950	4.94	0.1546	0.1546	0.0789	0.1578
1.100	1.100	7.92	0.1534	0.1534	0.0789	0.1580
1.290	1.290	14.38	0.1529	0.1529	0.0789	0.1578
2.060	2.060	161.61	0.1512	0.1512	0.0791	0.1582
3.280	3.280	7.4×10^3	0.1526	0.1526	0.0793	0.1587
3.830	3.830	4.2×10^4	0.1538	0.1538	0.0700	0.1601
4.470	4.470	3.1×10^5	0.1556	0.1556	0.0809	0.1618
7.130	7.130	1.3×10^9	0.1593	0.1593	0.0821	0.1643
8.330	8.330	5.8×10^{10}	0.1598	0.1598	0.0836	0.1672
9.720	9.720	4.5×10^{12}	0.1608	0.1608	0.0853	0.1705
11.360	11.360	7.9×10^{14}	0.1610	0.1610	0.0873	0.1746

*   High and low frequency impedance normalized to Z_0.

Table 5a.   Normalized effective rate of rise for non-planar conical wave launchers in a staggered asymmetric configuration; $l/\sqrt{A}$ = 1 and 2.

$\dfrac{b}{a}$	f_g *	$\dfrac{b''}{a''}$ (using (A.16))	$l/\sqrt{A} = 5$		$l/\sqrt{A} = 10$	
			$T_{n1}^{(asym)}$	$T_{n2}^{(asym)}$	$T_{n1}^{(asym)}$	$T_{n2}^{(asym)}$
1.51	1.51	28.71	0.0321	0.1603	0.0160	0.1603
1.76	1.76	62.97	0.0323	0.1614	0.0161	0.1614
2.06	2.06	161.61	0.0326	0.1631	0.0163	0.1631
2.40	2.40	470.27	0.0331	0.1656	0.0166	0.1656
2.81	2.81	1.7×10^3	0.0337	0.1689	0.0169	0.1689
3.28	3.28	7.4×10^3	0.0346	0.1728	0.0173	0.1728
3.83	3.83	4.2×10^4	0.0355	0.1777	0.0178	0.1777
4.47	4.47	3.1×10^5	0.0366	0.1832	0.0185	0.1846
5.22	5.22	3.3×10^6	0.0378	0.1893	0.0191	0.1909
6.10	6.10	5.2×10^7	0.0391	0.1957	0.0198	0.1978
7.13	7.13	1.3×10^9	0.0405	0.2027	0.0205	0.2051
8.33	8.33	5.8×10^{10}	0.0419	0.2098	0.0213	0.2128
9.72	9.72	4.5×10^{12}	0.0434	0.2171	0.0221	0.2207
11.36	11.36	7.9×10^{14}	0.0449	0.2265	0.0229	0.2288
13.27	13.27	3.1×10^{17}	0.0463	0.2318	0.0237	0.2370
15.50	15.50	3.5×10^{20}	0.0478	0.2389	0.0245	0.2454
18.10	18.10	1.2×10^{24}	0.0492	0.2461	0.0254	0.2538
21.15	21.15	1.8×10^{28}	0.0506	0.2528	0.0262	0.2622
24.70	24.70	1.2×10^{33}	0.0519	0.2596	0.0270	0.2705
28.85	28.85	5.7×10^{38}	0.0532	0.2659	0.0278	0.2787

*   High and low frequency impedance normalized to Z_0.

Table 5b.   Normalized effective rate of rise for non-planar conical wave launchers in a staggered asymmetric configuration; $l/\sqrt{A} = 5$ and 10.
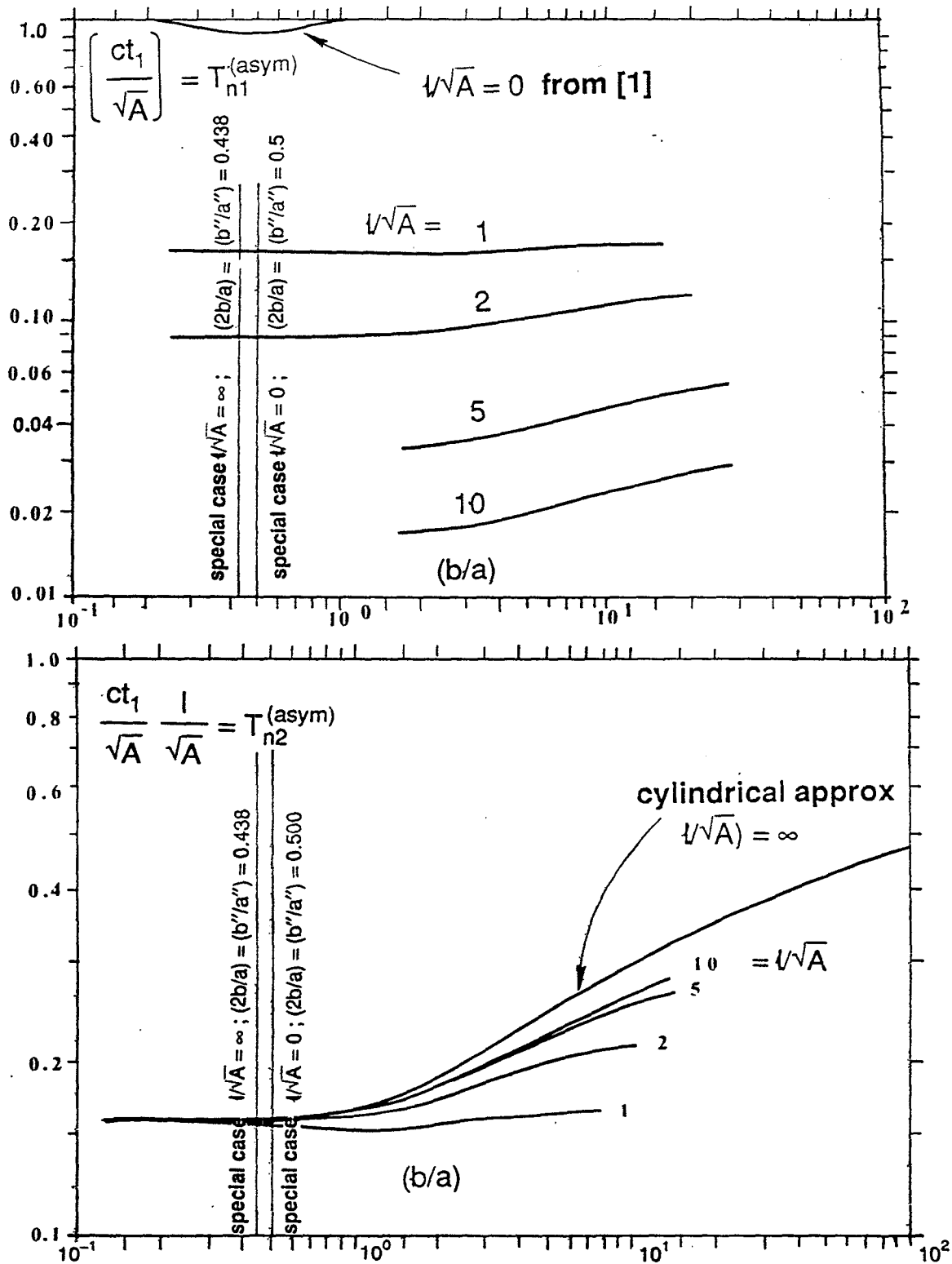
Figure A.10. Normalized effective rates of rise in the distant field along the normal direction for the asymmetric configuration

-43-

The tables and plots in this appendix are expected to be useful in designing an array of conical wave launchers in either symmetric or asymmetric configurations for specific values of a, b, t_1 etc. as required. It is noted that in practice, the flat plates could have rollups at their edges as needed and the effect of rollup has been studied by the authors [15]. In practical design, the widths of flat plates could account for the presence of rollups. Furthermore, it is important to recall that we have estimated the effective rate of rise in the far field assuming ideal step-function fields at all source points. In practice, the source-point field has finite rise time of course. In other words, the rises estimated here are only due to the electromagnetic effects of arraying, and by judicious choice of the geometrical parameters of the array, the "array rise time" can be minimized and perhaps be even made negligible compared to other physical mechanisms in the source contributing toward the rise time. However, one should be careful as l is increased, because at some point mutual interaction between the conical launchers may become significant and adversely influence the resulting radiated waveform.

References

1. C.E. Baum, "Early Time Performance at Large Distances of Periodic Planar Arrays of Planar Bicones with Sources Triggered in a Plane-Wave Sequence," Sensor and Simulation Note 184, 30 August 1973.

2. C.E. Baum, "EMP Simulators for Various Types of Nuclear EMP Environments: An Interim Categorization," Sensor and Simulation Note 240, January 1978 and Joint Special Issue on the Nuclear Electromagnetic Pulse, IEEE Transactions on Antennas and Propagation, January 1978, pp. 35-53, and IEEE Transactions on Electromagnetic Compatibility, February 1978, pp. 35-53.

3. C.E. Baum, "Some Characteristics of Planar Distributed Sources for Radiating Transient Pulses," Sensor and Simulation Note 100, 12 March 1970.

4. C.E. Baum, "The Distributed Source for Launching Spherical Waves," Sensor and Simulation Note 84, 2 May 1969.

5. C.E. Baum and D.V. Giri, "The distributed Switch for Launching Spherical Waves," Sensor and Simulation Note 289, 28 August 1985.

6. Y.G. Chen, S. Lloyd, R.Crumley, C.E. Baum and D.V. Giri, "Design Procedures for Arrays which Approximate a Distributed Source at the Air-Earth Interface," Sensor and Simulation Note 292, 1 May 1986.

7. W.R. Smythe, *Static and Dynamic Electricity*, 3rd ed., McGraw Hill, 1968.

8. C.E. Baum, "The Conical Transmission Line as a Wave Launcher and Terminator for a Cylindrical Transmission Line," Sensor and Simulation Note 31, 16 January 1967.

9. C.E. Baum, "Impedances and Field Distributions for Parallel Plate Transmission Line Simulators," Sensor and Simulation Note 21, 6 June 1966.

10. T.L. Brown and K.D. Granzow, "A Parameter Study of Two Parallel Plate Transmission Line Simulators of EMP Sensor and Simulation Note 21," Sensor and Simulation Note 52, 19 April 1968.

11. C.E. Baum, D.V. Giri and R.D. Gonzalez, "Electromagnetic Field Distribution of the TEM Mode in a Symmetrical Two-Parallel-Plate Transmission Line," Sensor and Simulation Note 219, 1 April 1976.

12. F.C. Yang and K.S.H. Lee, "Impedance of a Two-Conical-Plate Transmission Line," Sensor and Simulation Note 221, November 1976.

13. F.C. Yang and L. Marin, "Field Distributions on a Two-Conical-Plate and a Curved Cylindrical-Plate Transmission Line," Sensor and Simulation Note 229, September 1977.

14. T.L. Brown D.V. Giri and H. Schilling, "Electromagnetic Field Computation for a Conical Plate Transmission Line Type of Simulator," DIESES Memo 1, 23 November 1983.

15. D.V. Giri and C.E. Baum, "Equivalent Displacement for a High-Voltage Rollup on the Edge of a Conducting Sheet," Sensor and Simulation Note 294, 15 October 1986.